Michigan State University

National Superconducting Cyclotron Laboratory

THERMALIZATION IN NUCLEUS-NUCLEUS COLLISIONS

F. ZHU, W.G. LYNCH, D.R. BOWMAN, R.T. de SOUZA,
C.K. GELBKE, Y.D. KIM, L. PHAIR, M.B. TSANG,
C. WILLIAMS, H.M. XU, and J. DINIUS

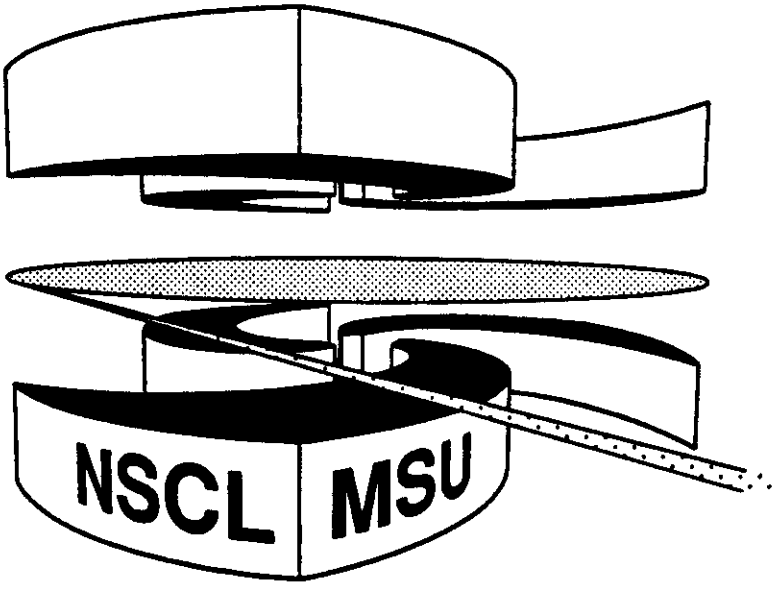

MSUCL-820 **JANUARY 1992**

MSUCL-820
January, 1992

Thermalization in Nucleus-Nucleus Collisions

F. Zhu, W.G. Lynch, D.R. Bowman, R.T. de Souza[†], C.K. Gelbke
Y.D. Kim[†], L. Phair, M.B. Tsang, C. Williams, H.M. Xu[tt], and J. Dinius,
Department of Physics and Astronomy and
National Superconducting Cyclotron Laboratory
Michigan State University, East Lansing, Michigan 48824

Abstract

Impact parameter dependent excited state populations of intermediate mass fragments are investigated for ^{36}Ar induced reactions on ^{197}Au at E/A=35 MeV. Population inversions, indicative of non-thermal excitation mechanisms, are observed in peripheral collisions characterized by low associated charged particle multiplicities. These population inversions disappear for collisions with larger associated charged particle multiplicities, consistent with a more complete thermalization for more complex final states. Discrepancies, observed in central collisions, suggest that the limit of local thermal equilibrium has not yet been observed.

PPACS index: 25.70 Np

In energetic nucleus-nucleus collisions, very hot and dilute nuclear systems can be created which decay on timescales commensurate with nuclear relaxation times.[1-5] These transient excitations offer singular opportunities for determining the statistical properties of hot nuclei [2,3] and hot nuclear matter.[4-8] Comparisons of such reactions to statistical theories are often based upon the assumption that the hot nuclear system attains local thermal equilibrium.[4,5] A recent test of this assumption, however, revealed non-thermal populations of the excited states of emitted intermediate mass fragments (Z=3-8), an effect most clearly manifested by inversions in the excited state populations of emitted ^{10}B fragments.[9,10] To investigate whether this observation may be related to the dominance of large impact parameter collisions by non-equilibrium transport phenomena,[11-14] we measured ^{10}B excited state populations in conjunction with a charged particle multiplicity filter.

The experiment was performed by bombarding a 1.0 mg/cm^2 ^{197}Au target with a 1260 MeV ^{36}Ar beam produced by the K500 cyclotron of the National Superconducting Cyclotron Laboratory of Michigan State University. The decays of particle unstable intermediate mass fragments (IMF's : Z=3-20) were detected by a tetragonal hodoscope of 13 telescopes,[15] centered at $\Theta_{lab} = 39°$. Nine telescopes, each having a solid angle of 3.6 msr, and consisting of an x-y position sensitive proportional counter, a planar 150 μm silicon surface barrier detector, a 5 mm lithium drift silicon detector, and a 400 μm silicon surface barrier veto counter, were used for the detection of light particles. The four remaining telescopes, each having a solid angle of 5.6 msr and consisting of an x-y position sensitive proportional counter, planar 75 and 100 μm thick surface barrier detectors, and a 5 mm lithium drift silicon detector, were used for the detection of intermediate mass fragments. Energy

calibrations, accurate to 1%, were obtained from an ^{241}Am source and a calibrated pulser.

The multiplicity of associated charged particles was measured with rings 2-11 of the MSU Miniball phoswich detector array, [16] which spanned polar angles of $16° \leq \theta \leq 160°$. To accommodate the hodoscope, 27 of the original 176 phoswich detectors of rings 2-11 were removed; the remaining array covered approximately 77% of 4π. Charged particles were identified by element for Z≈1-20 in the Miniball, with thresholds of 2, 3, and 4 MeV/nucleon for Z=3, 10, and 18 fragments, respectively. Further details of the Miniball detection array are provided in refs. [16,17].

Measured charged particle multiplicity distributions are shown in the upper right corner of Fig 1.[18] The solid points indicate the probability of observing the charged particle multiplicity, N_A, in the Miniball associated with the detection of a ^{10}B nucleus in the hodoscope. The dashed line indicates the corresponding inclusive multiplicity distribution.[18] The impact parameter scale in the figure was estimated by assuming a monotonic relation between the impact parameter and the associated multiplicity.[17] Consistent with previous observations,[17,19] the detection of one ^{10}B fragment in the hodoscope suppresses peripheral collisions significantly. Gates, indicated by the dashed-dotted lines, were used to distinguish "peripheral" ($N_A \leq 5$) and "central" collisions ($N_A \geq 10$) collisions. Energy spectra for particle stable ^{10}B fragments for these two multiplicity bins are shown in the remainder of Fig. 1. The spectra for central collisions have steeper slopes than those obtained for peripheral collisions, reflecting a more complete dissipation of the incident energy into other degrees of freedom.

The relative populations of particle unstable states in ^{10}B nuclei were measured by detecting the coincident decay products. These yields are shown as a function of excitation energy for the $^{10}B^{*} \rightarrow {}^{6}Li+\alpha$ and $^{10}B^{*} \rightarrow {}^{9}Be+p$ decay channels in the upper and lower halves of Fig. 2, respectively. Spectra obtained for peripheral and central collisions are shown in the left and right sides of the figure, respectively. The separation energy E_b for each decay channel and the locations and spins of the relevant particle unstable excited states of ^{10}B nuclei are indicated in the left hand panels of the figure.[20] In comparison to lower lying particle unbound states, the group of states at about 6 MeV excitation energy is more strongly populated in less violent "peripheral" collisions than in more violent "central" collisions.

The $^{6}Li+\alpha$ and $^{9}Be+p$ coincidence yields consist of a contribution, Y_c, from the decay of particle unstable ^{10}B nuclei into channel c and a background, Y_b. This background has been parameterized by [15]

$$Y_b = C_{12} Y_1 Y_2 \{1 - \exp[-(E^{*} - E_b)/\Delta_b]\}, \qquad (1)$$

where Δ_b governs the width of the minimum caused by the Coulomb repulsion between the two fragments; C_{12} is a fit parameter; and Y_1 and Y_2 are the measured inclusive yields for particles 1 and 2, gated by the appropriate charged particle multiplicity.

The measured yield $Y_c(E^{*})$ from the decay of particle unstable ^{10}B nuclei is related to the decay spectrum, $|dn(E)/dE|_c$, for decay into channel c by the equation

$$Y_c(E^*) = \int \varepsilon_c(E^*,E) \bullet \left|\frac{dn(E)}{dE}\right|_c \bullet dE. \qquad (2)$$

Here, $\varepsilon_c(E^*,E)$ is the efficiency of the hodoscope for detecting the decay products of particle unstable ^{10}B nuclei and E^* and E denote the measured and actual excitation energies,respectively. Details of the calculation of the efficiency function are provided in ref. [15].

The decay spectrum, $|dn(E)/dE|_c$ can be described for ^{10}B nuclei by a superposition of Breit-Wigner line shapes

$$\left|\frac{dn(E)}{dE}\right|_c = \sum_i n_i \frac{(2J_i+1)\Gamma_i/2\pi}{(E-E_i)^2+\Gamma_i^2/4} \bullet \frac{\Gamma_{c,i}}{\Gamma_i}, \qquad (3)$$

where n_i, E_i, Γ_i, and $\Gamma_{c,i}/\Gamma_i$, are the population probability, centroid, width, and branching ratio of the i-th state. The population probabilities, n_i, were extracted by fitting the coincidence yield, for different assumptions of the background parameter Δ_b. Reasonable fits were obtained for backgrounds lying within the values bounded by the dashed lines in Fig. 2. The population probabilities, n_i, were assumed to be the same within those groups of states in Fig. 2 which where not resolved. The best fits to the coincidence yields, are shown by the solid curves in Fig. 2.

Figure 3 shows the measured population probabilities as a function of excitation energy for peripheral (left side) and central (right side) collisions. The error bars include the uncertainties in the background subtraction bounded by the two assumed background coincidence yields displayed in Fig. 2. In thermal as well as many statistical models, the initial excited state population probabilities of intermediate mass fragments should be proportional to a Boltzmann factor, $\exp(-E^*/T_{eff})$ where T_{eff}

is the effective temperature of the system at breakup. The dashed lines in Fig. 3 show the exponential dependence dictated by the Boltzmann factor for $T_{eff} = 4$ MeV. For peripheral collisions, the measured relative populations deviate significantly from the expected monotonic behavior and a population inversion is observed; the group of states at E^{*} =6.0 MeV is populated much more strongly than the lower lying states at 5.2 and 4.8 MeV. Such effects were already observed in the inclusive measurements of ref. [9]. The inversions disappear for central collisions. The population probabilities, however, do not fall off exponentially as expected from the Boltzmann factor; instead, one observes an approximately constant population probability for the 5.2 and 6.0 MeV levels.

The initial populations of excited states will be modified by the sequential feeding from heavier particle unstable nuclei. These feeding corrections have been estimated via calculations in which it is assumed that the excited states of primary emitted fragments are populated thermally; the initial elemental yields are subject to a constraint that the final elemental distributions are consistent with the measured elemental distributions.[9,10] In these calculations, decays were calculated from the Hauser-Feshbach theory[21] with parity and isospin conservation taken into account; known branching ratios[22] were used when available. Unknown spins or parities of low lying discrete states were assigned randomly and calculations repeated with different spin assignments until sensitivities of the population probabilities to these uncertainties could be assessed.

In order to provide an overall comparison between the calculated and measured population probabilities, a least squares analysis was performed by computing

$$X^{2}_{\nu}(T) = \frac{1}{\nu} \sum_{i=1}^{\nu} \frac{(n_{exp,i} - n(T)_{cal,i})^{2}}{\sigma^{2}_{exp,i} + \sigma^{2}_{cal,i}}, \qquad (4)$$

for a range of initial emission temperatures. Here, $n_{exp,i}$ and $n(T)_{cal,i}$ are the measured and calculated population probabilities and $\sigma_{exp,i}$ and $\sigma_{cal,i}$ are the corresponding uncertainties. The resulting values of $X^2_\nu(T)$ are shown in table 1. Optimal agreement between calculated and measured population probabilities is obtained for both central and peripheral collisions at temperatures of about T ≈ 3-5 MeV. Similar residue temperatures have been obtained in dynamical [23,24] and in statistical [25-28] calculations. For T = 4 MeV, the population probabilities obtained by the sequential decay calculations are indicated by the open bars in the Fig. 3; the vertical extent of the bars graphically demonstrates the range of theoretical values obtained for ten randomly chosen assumptions about the unknown spins of low lying discete states. (Rotational effects may add comparable contributions to the uncertainties in the calculated population probabilities.[10]) The population probabilities obtained from the sequential decay calculations cannot be reconciled with the population inversions observed for peripheral collisions. For central collisions, on the other hand, the discrepancies between calculated and measured population probabilities are much smaller, but still too large for a purely thermal interpretation.

At present, there is no definitive explanation for enhanced populations of specific states like those contained in the group at E^* = 6 MeV. Such effects can arise from non-statistical population mechanisms or from statistical feeding which is governed by branching ratios that differ significantly from those assumed in the Hauser-Feshbach model.[10] The experimental trends in Fig. 3 suggest that such effects diminish as the number of alternative decay paths increase.

In summary, the impact parameter dependence of excited state populations of intermediate mass fragments has been investigated with a 4π charged particle array. A strong population inversion, indicative of non-thermal excitation mechanisms, is

observed in peripheral collisions characterized by low associated charged particle multiplicities. This population inversion largely disappears for central collisions, consistent with a trend towards greater thermalization as the complexity of the breakup configuration is increased. The remaining discrepancies observed in central collisions suggest that the limit of local equilibrium has not yet been observed.

This manuscript is based upon work supported by the National Science Foundation under Grant number PHY-89-13815. W.G. Lynch acknowledges the receipt of a U.S. Presidential Young Investigator Award.

† Present address: Indiana University Cyclotron Facility, 2401 Milo B. Sampson Lane, Bloomington IN 47405

†† Present address: Cyclotron Institute, Texas A&M University, College Station TX 77843-4242.

References

1. C.K. Gelbke, and D.H. Boal, Prog. Part. Nucl. Phys. 19 (1987) 33, and references contained therein.
2. E. Suraud, C. Grégoire, and B. Tamain, Prog. Part. Nucl. Phys. 23 (1989) 357, and references contained therein.
3. D. Guerreau, "Nuclear Matter and Heavy Ion Collisions", Plenum Press, Nato ASI Series B 205 (1989) 187, and references contained therein.
4. L.P. Csernai, and J.I. Kapusta, Phys. Rep. 131 (1986) 223, and references contained therein.
5. W.G. Lynch, Ann. Rev. Nucl. Part. Sci. 37 (1987) 493, and references contained therein.
6. R.T. de Souza, L. Phair, D.R. Bowman, N. Carlin, C.K. Gelbke, W.G. Gong, Y.D. Kim, M.A. Lisa, W.G. Lynch, G.F. Peaslee, M.B. Tsang, H.M. Xu, and F. Zhu, Phys. Lett. B 268 (1991) 6.
7. D.R. Bowman, G.F. Peaslee, R.T. de Souza, N. Carlin, C.K. Gelbke, W.G. Gong, Y.D. Kim, M.A. Lisa, W.G. Lynch, L. Phair, M.B. Tsang, C. Williams, Phys. Rev. Lett. 67 (1991) 1527.
8. C.A. Ogilvie, J.C. Adloff, M. Begemann-Blaich, P. Bouissou, J. Hubele, G. Imme, I. Iori, P. Kreutz, G.J. Kunde, S. Leray, V. Lindenstruth, Z. Liu, U. Lynen, R.J. Meijer, U. Milkau, W.F.J. Müller, C. Ngô, J. Pochodzalla, G. Raciti, G. Rudolf,

H. Sann, A. Schüttauf, W. Seidel, L. Stuttge, W. Trautmann, and A. Tucholski, Phys. Rev. Lett. 67 (1991) 1214.

9. T.K. Nayak, T. Murakami, W.G. Lynch, K. Swartz, D.J. Fields, C.K. Gelbke, Y.D. Kim, J. Pochodzalla, M.B. Tsang, H.M. Xu, F. Zhu, and K. Kwiatkowski, Phys. Rev. Lett. 62 (1989) 1021.
10. T.K. Nayak, T. Murakami, W.G. Lynch, K. Swartz, D.J. Fields, C.K. Gelbke, Y.D. Kim, J. Pochodzalla, M.B. Tsang, H.M. Xu, F. Zhu, and K. Kwiatkowski, Phys. Rev. C45, 132.
11. T.C. Awes, R.L. Ferguson, R. Novotny, F.E. Obenshain, F. Plasil, S. Pontoppidan, V. Rauch, G.R. Young, and H. Sann, Phys. Rev. Lett. 52 (1984) 251.
12. R. Vandenbosch, A. Lazzarini, D. Leach, D.K. lock, A. Ray, and A. Seamster, Phys. Rev. Lett. 52 (1984) 1964.
13. J. Randrup, Nucl. Phys. A307 (1978) 319; A327 (1979) 490.
14. T. Døssing and J. Randrup, Nucl. Phys. A433 (1985) 215; A433 (1985) 280.
15. T. Murakami, T.K. Nayak, W.G. Lynch, K. Swartz, Z. Chen, D.J. Fields, C.K. Gelbke, Y.D. Kim, M.R. Maier, J. Pochodzalla, M.B. Tsang, H.M. Xu, and F. Zhu, Nucl. Instr. and Meth. A275 (1989) 112.
16. R.T. DeSouza, N. Carlin, Y.D. Kim, J. Ottarson, L. Phair, D.R. Bowman, C.K. Gelbke, W.G. Gong, W.G. Lynch, R.A. Pelak, T. Peterson, G. Poggi, M.B. Tsang, and H.M. Xu, Nucl. Instr. and Meth. A295 (1990) 109.
17. Y.D. Kim, R.T. de Souza, D.R. Bowman, N. Carlin, C.K. Gelbke, W.G. Gong, W.G. Lynch, L. Phair, M.B. Tsang, and F. Zhu, Phys. Rev. C. in press.
18. This is the multiplicity detected in the 149 active Miniball elements, not the multiplicity [17] which would be detected in the complete array.
19. Y.D. Kim, M.B. Tsang, C.K. Gelbke, W.G. Lynch, N. Carlin, Z. Chen, R. Fox, W.G. Gong, T. Murakami, T.K. Nayak, R.M. Ronningen, H.M. Xu, F. Zhu, W.

Bauer, L.G. Sobotka, D. Stracener, D.G. Sarantites, Z. Majka, V. Abenante, and H. Griffin, Phys. Rev. Lett. 63 (1989) 494.

20. Additional states at E^* = 7.67, 7.819, 8.07, 8.7, 8.889 and 8.895 MeV were included in the fit, but were characterized by populations which were statistically insignificant, though consistent with an emission temperature of about 4 MeV. The structure at 7 MeV in the ^{9}Be+p spectrum reflects contributions from excited states at 6.873 and 7.002 MeV which have poorly known proton branching ratios, superimposed upon a prominent peak in the detection efficiency of the hodoscope.
21. W. Hauser and H. Feshbach, Phys. Rev. 87 (1952) 366.
22. F. Ajzenberg-Selove, Nucl. Phys. A475 (1987) 1; A413 (1984) 1; A433 (1985) 1; A449 (1986) 1; A460 (1986) 1.
23. H.M. Xu, P. Danielewicz, and W.G. Lynch, to be published.
24. D. Boal, J. Glosli, and C. Wicentowich, Phys. Rev. C40 (1989) 601.
25. S. Levit and P. Bonche, Nucl. Phys. A437 (1984) 426.
26. D.H.E. Gross, Phys. Lett. B203 (1988) 26.
27. J.P. Bondorf, R. Donangelo, L.N. Mishustin, C.J. Pethick, H.Schulz and K. Sneppen, Nucl. Phys. A443 (1985) 321.
28. W.A. Friedman, Phys. Rev. Lett. 60 (1988) 2125.

Captions

Table 1: Values for $\chi^2_\nu(T)$ are calculated, according to Eq. 4, for temperatures ranging from 2 to 6 MeV.

Fig. 1: Energy spectra for ^{10}B nuclei detected at 45° in the high resolution hodoscope, for low multiplicity (solid points) and high multiplicity (solid squares) gates on the Miniball. The solid lines denote moving source fits, used in the efficiency calculations. The solid points (connected by a solid curve) in the insert are the measured probability distribution for the associate multiplicity of charged particles in coincidence with ^{10}B nuclei detected in the high resolution hodoscope. The dashed line depicts the inclusive multiplicity distribution, normalized arbitrarily. The dashed-dotted lines depict the boundaries of the multiplicity gates described in the text.

Fig. 2: Yields for the decays: $^{10}B \rightarrow {}^{6}Li + \alpha$ (upper half) and $^{10}B \rightarrow {}^{9}Be + p$ (lower half). Spectra obtained for peripheral and central collisions are shown on the left and right hand sides, respectively. The curves are described in the text.

Fig. 3: The solid points designate population probabilities for the excited states of ^{10}B nuclei measured for peripheral (left side) and central (right side) collisions. The open bars indicate the results of the sequential decay calculations. The solid lines denote exponentials $\exp(E^*/T_{eff})$ with $T_{eff} = 4$ MeV.

T (MeV)	χ^2_ν(Peripheral)	χ^2_ν(Central)
2	55.5	30.3
3	14.2	3.14
4	10.3	2.41
5	9.35	2.77
6	17.5	7.12

Table 1

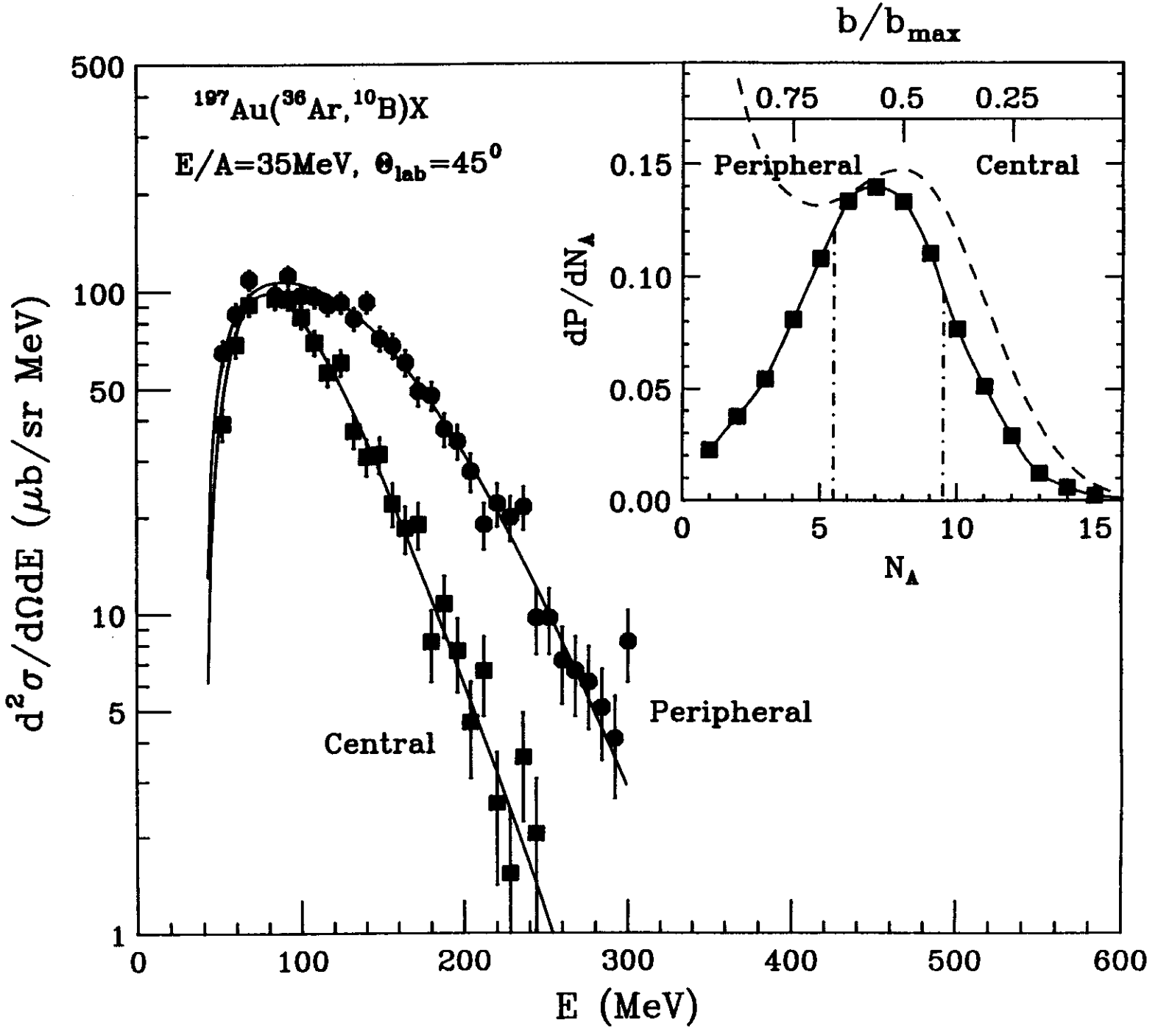
b/b_max
0.75
0.5
0.25
Peripheral
Central
dP/dN_A
0.15
0.10
0.05
0.00
0
5
10
15
N_A
197Au(36Ar, 10B)X
E/A=35MeV, θ_lab=45°
d²σ/dΩdE (μb/sr MeV)
500
100
50
10
5
1
Central
Peripheral
0
100
200
300
400
500
600
E (MeV)

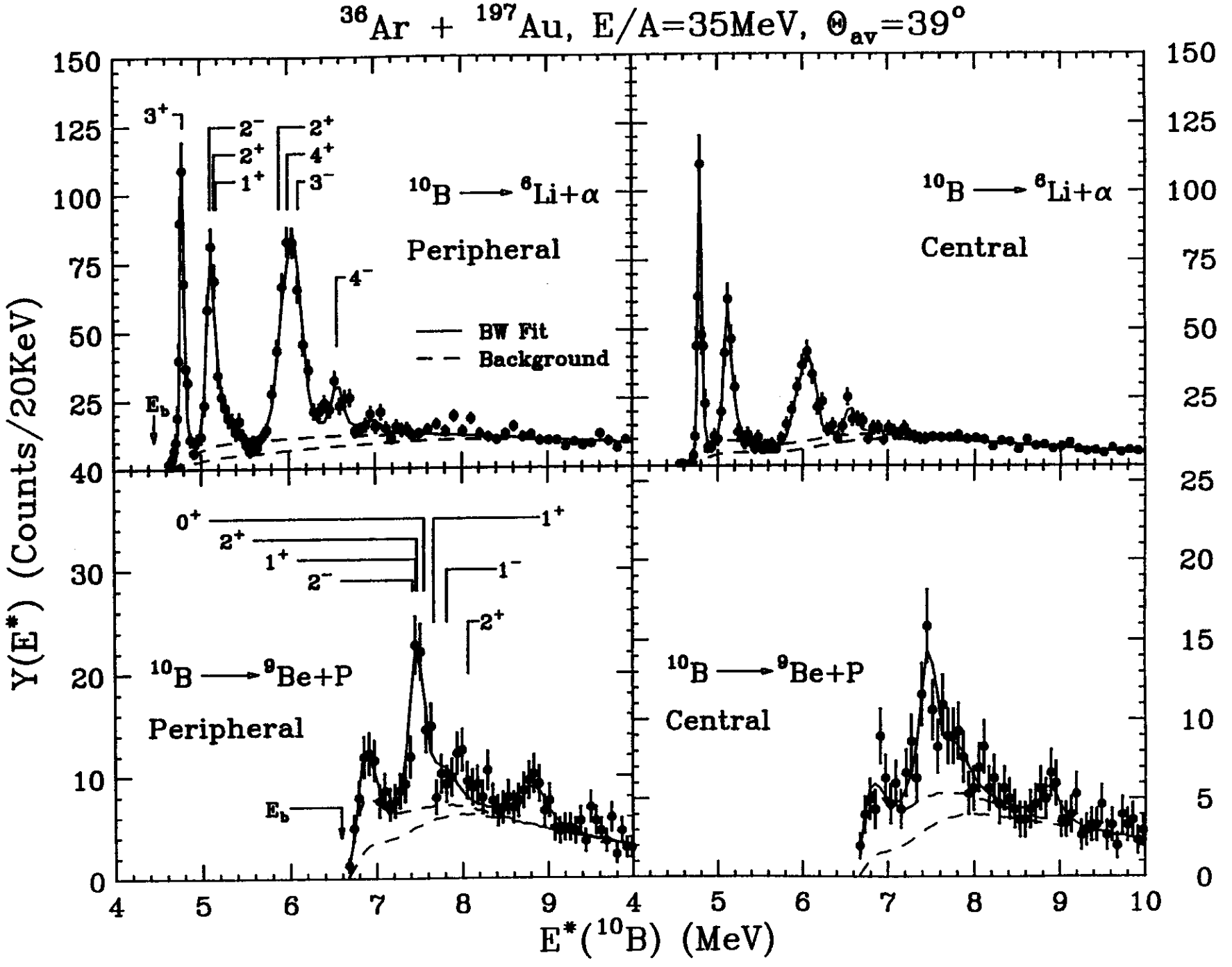
^{36}Ar + ^{197}Au, E/A=35MeV, Θ_{av}=39°
^{10}B → ^{6}Li+α
Peripheral
Central
BW Fit
Background
^{10}B → ^{9}Be+P
Peripheral
Central
Y(E*) (Counts/20KeV)
E*(^{10}B) (MeV)
E_b

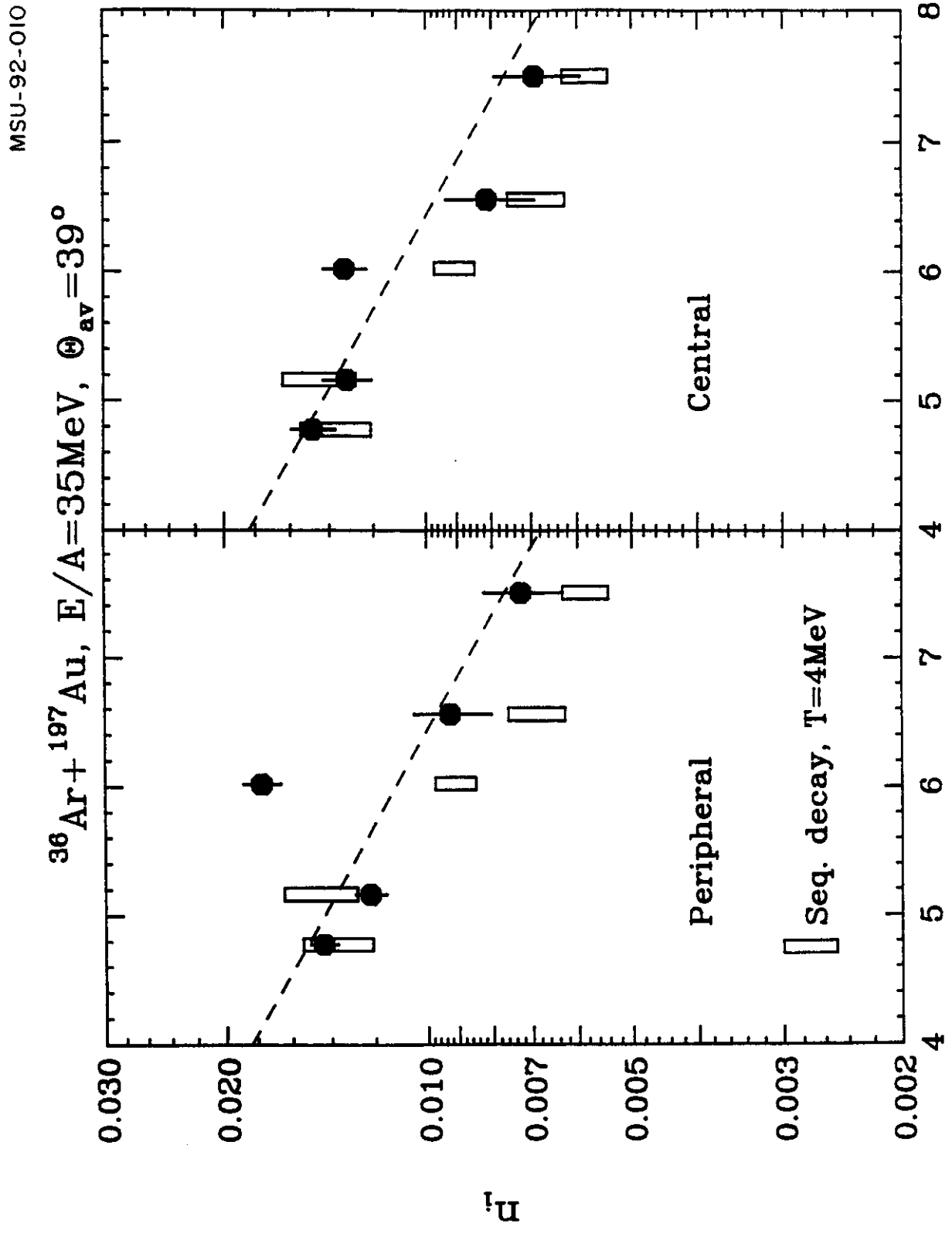
MSU-92-010
$^{36}Ar+^{197}Au$, E/A=35MeV, Θ_{av}=39°
Central
Peripheral
Seq. decay, T=4MeV
n_i
0.030
0.020
0.010
0.007
0.005
0.003
0.002
4
5
6
7
8
$E^*(^{10}B)$ (MeV)

Fig. 3